COBEM 2023 27TH INTERNATIONAL CONGRESS OF MECHANICAL ENGENEERING

ABCM Brazilian Society of Mechanical Sciences and Engineering
27th ABCM International Congress of Mechanical Engineering
December 04-08, 2023, Florianópolis-SC, Brazil

COB-2023-0352
ASSESSMENT OF TRUSS-BASED MODULAR STRUCTURES IN THE WINGBOX STRUCTURAL DESIGN OF COMMERCIAL AIRCRAFT

Pedro Davim Bastos
Higor Luis Silva
Federal University of Uberlândia, Faculty of Mechanical Engineering, Uberlândia-MG, 38408-100, Brazil
pedrodavim@ufu.br, higor@ufu.br

Abstract. *Disruptive projects and technologies have been presented with the aim of improving and reducing structural weight during aircraft design. With the replacement of fossil fuel by electric propulsive systems, and consequently with the removal of fuel tanks from the wing's inner structure, it is possible to rethink and develop new ways to optimize and reduce its weight. Therefore, based on the Common Research Model's wingbox, this work aims to showcase the effectiveness of a truss-based inner structure in fulfilling this objective in commercial aircraft, bringing a new structural design approach, where the conventional inner structures, such as ribs, spars, and stringers are replaced solely by a truss-based structure, and its joints are represented by mass elements. The static analysis of the structure is performed using a solver with NASTRAN, which in turn is integrated into a particle swarm optimization that will optimize the design variables of the optimization problem. Design variables include the outer radius and thickness of each truss element of the structural mesh. The possibility of removing unnecessary elements is also evaluated, while still ensuring the minimum aerodynamic profile necessary to form the wing. The wingbox structure is then optimized in search of the lowest structural weight considering stress constraints. The results, verified by a buckling post-analysis, show that truss-based modular structures can be a good strategy in structural wing designs, in terms of modularity and reduction of weight.*

Keywords: *wing design, aircraft structures, optimization.*

1. INTRODUCTION

The concept of minimizing an aircraft's empty weight, although essential, is not entirely new in the aeronautical industry. Since the beginning of its relatively short but intense history, reducing the aircraft's empty weight has always been a priority. This is because reducing weight directly correlates with lower fuel consumption and, consequently, decreased operational costs. However, in recent times, the aeronautical industry has also started addressing new concerns with great urgency, such as environmental impacts. The industry aims to emit fewer pollutants and reduce noise emissions (Masiol and Harrison, 2014; Graham *et al.*, 2014). As a result, research focus has shifted towards alternative propulsion systems, replacing conventional fossil fuel-based engines with hydrogen cells and hybrid-electric systems (Friedrich and Robertson, 2015; Petrescu *et al.*, 2020; Pornet and Isikveren, 2015). Nonetheless, optimizing an aircraft's empty weight remains central to these studies (Silva *et al.*, 2021; Sgueglia *et al.*, 2020).

The wing design plays a critical role in the structural weight of an aircraft. Given that, optimizing wing performance and its wingbox's empty weight are key concepts in minimizing an aircraft's empty weight. Throughout the history of the aeronautical industry, several attempts have been made in order to achieve these goals, such as aeroelastic tailoring of wings using curvilinear stiffeners (Stanford and Jutte, 2017; Jutte *et al.*, 2014) and composites (Stanford *et al.*, 2014; Guimarães *et al.*, 2017), or the structural design of wings accounting for buckling constraints (Guimarães *et al.*, 2019; Starnes Jr and Haftka, 1979). Additionally, as the industry shifts towards replacing fossil fuel-based engines and removing fuel tanks, there is an opportunity to redesign the inner volume of the wingbox and explore alternative optimized structural arrangements to minimize weight. Recent studies (Silva *et al.*, 2023; Coggin *et al.*, 2014) have combined these concepts with an innovative approach: a wingbox with truss-based modular structures. Even though modular wing structures may be associated with morphing wings (Finistauri *et al.*, 2012; Tang *et al.*, 2016), in this case, conceptually, it involves the replacement of the internal structure of a traditional wingbox (ribs, spars and stringers) by a truss-based structure. Then, the trusses are responsible for providing all the needed structure integrity of the wingbox and, consequently, most of its empty weight.

Historically, the B-17 Flying Fortress' structural project followed this approach, with an "N" truss pattern as its wing's spars and ribs (Aerovintage, 2022) Its glaring issue was put in the spotlight in April 2021, with the temporary grounding of all remaining B-17s, whereupon the wing-fuselage attach structure, more specifically its left forward terminal fittings where bolted into the wing spar chord, in which the joint separated and allowed the wing to shift two inches at the attach point. Even though Airworthiness Directive (AD) 2034-10-04 allowed for the ungrounding of the B-17s, given the completion of its procedure, the significance of this problem, dating all the way back to AD 77-17-11 (January 1979), results

in conservative thoughts concerning to truss-based cantilever wing aircrafts. However, new manufacturing technologies, such as truss braced wings (TBW) may allow to bypass this problem, while even enhancing aircraft performance, specially with advancements made by some studies (Gern *et al.*, 2001; Bhatia *et al.*, 2009, 2012; Mallik *et al.*, 2013), displaying the effectiveness of the TBW. Other significant advancements include (Ye *et al.*, 2021; Bai and Yang, 2013) using additive manufacturing and fiber reinforced polymers in order to optimize the manufacturing of the trusses' joints.

This work aims to implement the concept of a truss-based modular internal wingbox structure into a large-scale model suitable for research purposes. The prototype chosen for this implementation is NASA's Common Research Model wingbox. The first step involves replacing the internal structure of the wingbox with a truss-based structure. Mass elements will represent the joints between trusses and skins, which will also be utilized for future buckling and aeroelastic optimizations. Boundary conditions will be established based on the wing-fuselage connection constraints, and the loads will be determined using an aerodynamic model. Once the structure and boundary conditions are defined, the integration of a single-objective particle swarm optimization and NASTRAN will be employed to optimize the wingbox mass. This optimization process will consider the discrete outer radius and thickness of each individual truss element, focusing on key structural responses such as total displacement and stress on the truss-based structures. Additionally, unnecessary truss elements that do not contribute to maintaining the minimum aerodynamic profile can be removed. Finally, a post-analysis on buckling will be conducted using NASTRAN SOL106 to ensure the structural integrity of the wingbox.

2. MODEL DESCRIPTION

2.1 Structural Model

The NASA Common Research Model (CRM) is an open-source aircraft geometry that was developed in 2007-2008 through a partnership between NASA, Boeing, and other industry and government groups for the validation and assessment of computational-fluid-dynamics (CFD) tools (Vassberg *et al.*, 2008). Over the years, it has been used by many researchers in different studies (Rivers, 2019; Lacy and Sclafani, 2016; Rivers *et al.*, 2019).

The CRM geometry is representative of a typical wide-body transonic transport aircraft (Figure 1). Primarily, the CRM wing has a wingspan of b = 58.76 m and an aspect ratio of AR = 9, resulting in a total wing area of S = 412.7 m^2. The reference area is S_{ref} = 383.74 m^2 and the exposed wing area is S_{exp} = 337.05 m^2. The wing is double tapered with a break at 37% semispan and a taper ratio of λ = 0.533 inboard of the break and λ = 0.376 outboard of the break, whilst its reference chord is c_{ref} = 7.01 m. Additionally, the CRM wing is designed for cruising at a Mach number of 0.85, at an altitude of 35000 ft (10668 m), and a lift coefficient of C_L = 0.5. Under standard atmospheric conditions with no temperature offset, this corresponds to a Reynolds number of approximately Re = 4.3 $\times$ 10^7. The wing and flight reference values are summarized in Table 1.

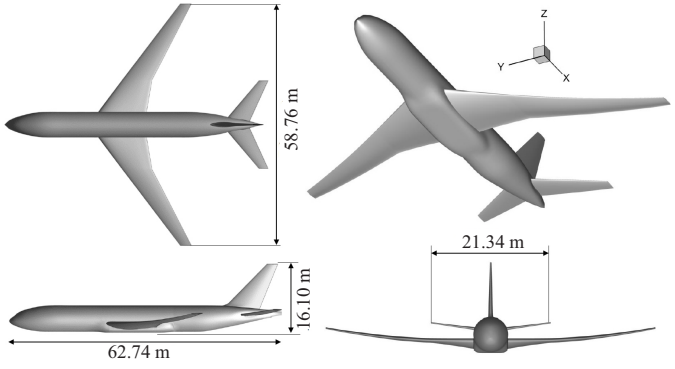

Figure 1: CRM views. Source: Fujiwara *et al.* (2018)

Table 1: Wing and flight parameters for the CRM.

Parameter	Value
Wingspan, b	58.76 m
Aspect ratio, AR	9.00
Total wing area, S	412.70 m^2
Reference area, S_{ref}	383.74 m^2
Exposed wing area, S_{exp}	337.05 m^2
Reference chord, c_{ref}	7.01 m
Altitude	10668 m
Mach number	0.85
Lift coefficient	0.50
Reynolds number	4.3 $\times$ 10^7

As a common reference and baseline, the structural model was based on the CRM's Finite Element Model (FEM) designed on NASTRAN, more specifically its twelfth coarse version, which was retrieved from Vassberg (2012). Figure 2 depicts the FEM model of the wingbox, while Table 2, the model's properties, in which both the wingbox's internal structure - of ribs, spars and stringers - and skin elements are modeled as plate elements. Then, its internal structure is replaced by a truss-based modular structure, represented by bar elements, due to their availability in a buckling analysis, while maintaining the same main dimensions of the CRM's wingbox, such as rib spacing and aerodynamic profile. Alternating "N" truss patterns are used in the ribs (Figure 7) and between them, in three different positions, parallel to the upper skin (Figure 3a), parallel to the lower skin (Figure 3b) and parallel to the wingbox's height (Figure 3c). The pattern is inspired by the aforementioned B-17 truss-based ribs and spar pattern, with the alternation from rib to rib inspired by Silva *et al.* (2022). It is worth mentioning that the number of sections between the ribs depends on the rib's chord, taking

maximum value of 8 at wing root and minimum value of 3 at wing tip.

Furthermore, to account for the joints between trusses, mass elements of 150 g are placed at each node of the model, following the approach proposed by Silva *et al.* (2022). Skin panels were added onto the external surface, represented by plate elements, aiming for representativity in both the static and buckling analysis. Finally, the truss-based CRM FEM is displayed in Figure 4 and its properties are available in Table 3. It is worth noting that all trusses and skin panels had the mesh size of their original geometry, being that the curve or surface, in order to minimize computational cost in the optimization process, with that accounting for the coarse mesh of the truss-based model when compared to the original one.

Table 2: Original FEM properties.

Property	Amount
Nodes	6687
Internal elements	7030
Ribs	52
Skin elements	1129
Mass elements	20

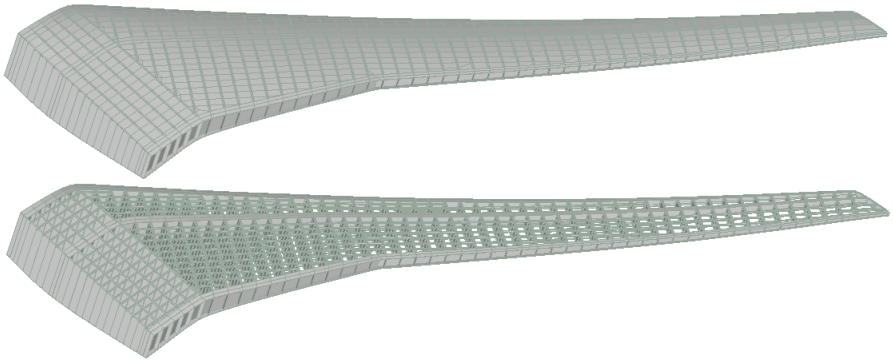

Figure 2: FEM of the original NASA CRM on NASTRAN.

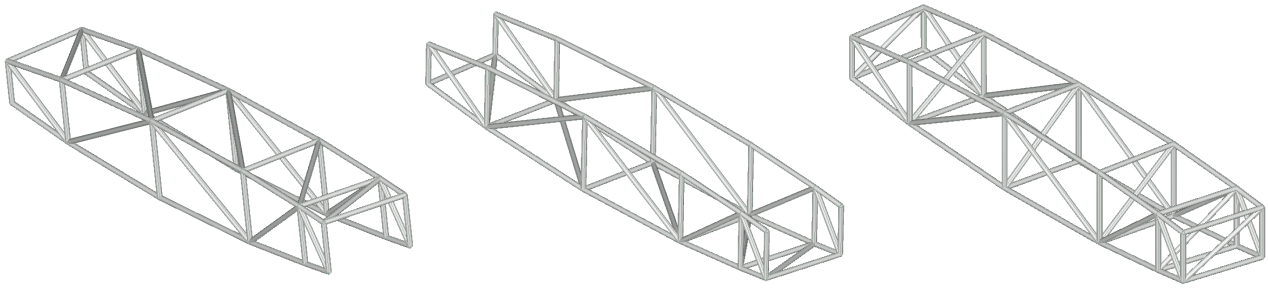

(a) Parallel to the upper skin. (b) Parallel to the lower skin. (c) Parallel to the wingbox's height.

Figure 3: Truss patterns.

Table 3: Truss FEM properties.

Property	Amount
Nodes	762
Truss elements	3183
Truss Ribs	52
Skin elements	600
Mass elements	710

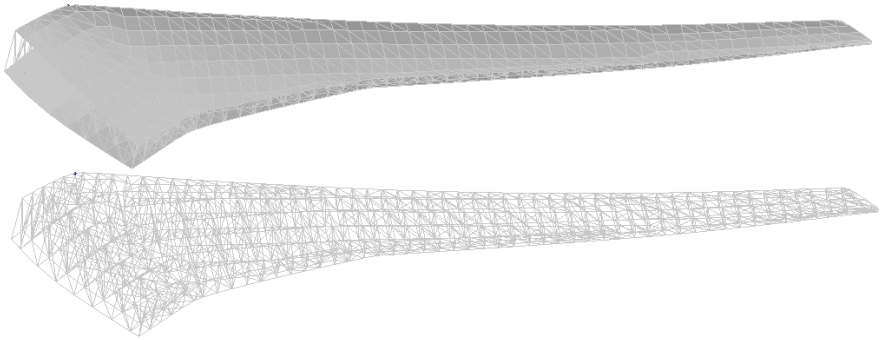

Figure 4: Finite element model of the truss-based NASA CRM on NASTRAN.

Moreover, the material properties for the carbon fiber laminate plate, used in the skin panels, are displayed in Table 4. Meanwhile, carbon fiber tubes, used in the trusses, were modeled as an isotropic material, since these are majorly submitted to loads in the axial direction of their structures and, since they behave similarly to a fragile material, the

maximum traction/compression stresses were used as their failure indices. Hence, the material properties for the carbon fiber tube, used in the trusses, are displayed in Table 5. It is worth mentioning that, with the use of composites, also comes the necessity to evaluate the propagation of parametric uncertainties, related to production and manufacturing defects, which may negatively affect the composite's properties (Guimaraes *et al.*, 2017; Mesogitis *et al.*, 2014). However, since this is not the focus of this study, the manufacturing will be assumed as ideal, with the mechanical properties displayed maintained with the manufacturing.

Table 4: Carbon fiber laminate plate properties.

Property	Value	Property	Value
E_1	98 GPa	T_1	1314 MPa
E_2	7.9 GPa	C_1	1220 MPa
ν_{12}	0.28	T_2	43 MPa
G_{12}	5.6 GPa	C_2	168 MPa
Density	1520 kg/m^3	S_{12}	48 MPa

Source: Stanford *et al.* (2014)

Table 5: Carbon fiber tube properties.

Property	Value
E	180 GPa
ν	0.28
Limit stress tension	550 MPa
Density	1650 kg/m^3

Source: EXEL EXELITE^{TM} Datasheet

Furthermore, the boundary conditions for the new FEM needed to be determined. The constraints from the original FEM were applied, where all degrees of freedom of each node in the wing-fuselage connection were clamped, while the loads applied were determined using the aerodynamic model described in more details in Subsection 2.2 Finally, having the FEM fully developed with its structure and boundary conditions determined, NASTRAN SOL101 was initially used in the optimization process (Section 3), with NASTRAN SOL106 used in a post-analysis (Subsection 4.3).

2.2 Aerodynamic Model

In order to develop the aerodynamic model, the CRM's performance and geometric properties were gathered and displayed in Tables 6 and 7, respectively, based on the information provided by Vassberg (2012) and Kenway *et al.* (2014). Additionally, the airfoil used in the model was the blunt tail-end (BTE) version of the CRM.65, which is depicted in Figure 5.

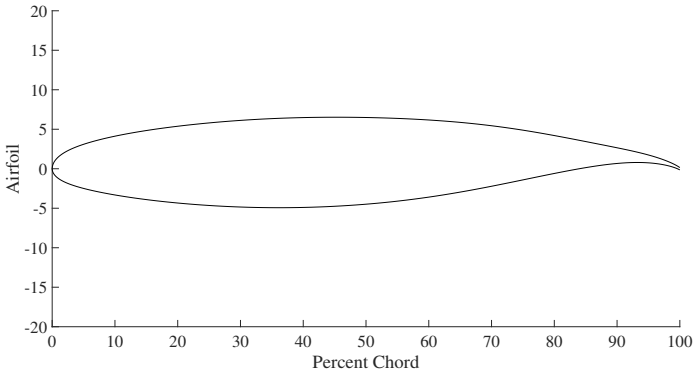

Figure 5: CRM.65 BTE airfoil.

Table 6: Performance properties of the NASA CRM.

Property	Value
Maximum takeoff weight	500000 lbs
Cruise height	35000 ft
Cruise Mach Number	0.85
Cruise speed	490 knots
Cruise load factor	1.16
Wing weight	30.29 ton

Table 7: Geometric properties of the NASA CRM.

Property	Value
Fuselage width	4.53 m
Semi-wingspan	29.38 m
End of first section semi-wingspan	12.44 m
Wing root chord	12 m
End of first section chord	6.12 m
Wing tip chord	2.4 m
Root-tip sweep wingbox angle	30°
Root-tip dihedral angle	8°
Airfoil profile	CRM.65 BTE

The aerodynamic model developed in this subsection is based on a fixed-speed horseshoe vortex analysis, specifically the Vortex Lattice Method (VLM1). It focuses primarily on the wing of the CRM and, given the aforementioned inputs, the aerodynamic model, including its panels, is presented in Figure 6. Based on the outputs from the fixed-speed VLM1 analysis, the total lift coefficient, lift, and twisting moment are distributed across the truss-based ribs of the wing, with the resulting loads applied at the aerodynamic center of each rib. It is worth noting that, in the structural model, an RBE3 element is used in order to represent the load application that results from the aerodynamic model, as displayed in Figure 7.

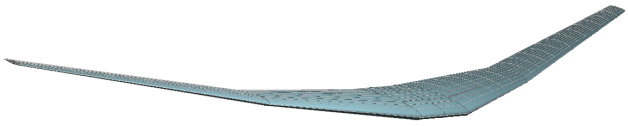

Figure 6: Aerodynamic model.

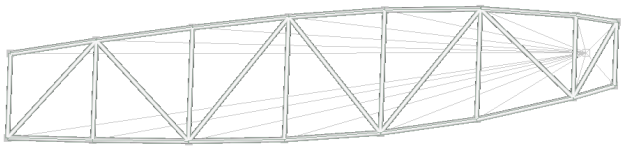

Figure 7: RBE3 element for load application at 25% wing chord.

3. OPTIMIZATION PROCESS

This work consists of a single-objective optimization, aiming to minimize the structural weight of the wingbox. As discussed in Subsection 2.1, the optimization is integrated with NASTRAN. Thus, an in-house algorithm writes the code with the required information to run SOL101 on NASTRAN. Then, the combined stresses in the trusses are determined, and they are considered the main optimization constraints. Given that, if a bar element surpasses its material's limit stress (considering a Factor of Safety of 1.5), it is proportionally penalized, i.e., it is penalized as much as it surpasses the allowed limit.

Initially, three different optimization methods were used: Differential Evolution, Genetic Algorithm, and Particle Swarm Optimization. The former as proposed by Cavalini Jr *et al.* (2016) and the others are the conventional built-in function available on MATLAB. After running some samples, the latter proved to consistently converge quicker and into a better result, while surpassing local optimal results. Thus, it was solely maintained for the rest of the work.

The design variables include the thickness and outer radius of each element. Throughout the optimization, the algorithm generates a population of different individuals with a variety combination of truss elements, which are evolved over the optimization in each generation. It is worth noting that the wingbox was structurally divided into 10 different sections, with the first one including the first 8 truss-based ribs and the rest including sequencing 5 truss-based ribs each, aiming for a different maximum and minimum outer radius and thickness for each section, given the expected structural response.

Additionally, the algorithm includes the removal of elements considered unnecessary for the structural response by the optimization. Nevertheless, the minimum elements necessary to guarantee the wingbox aerodynamic profile is ensured. Very thin elements are also removed from the optimization, which are the trusses with thicknesses smaller or equal to 10% of their outer radius.

Finally, after running SOL101 and considering the penalization of failed trusses, the final wingbox empty weight can be considered as the objective function for the optimization. The optimization flowchart is depicted in Figure 8.

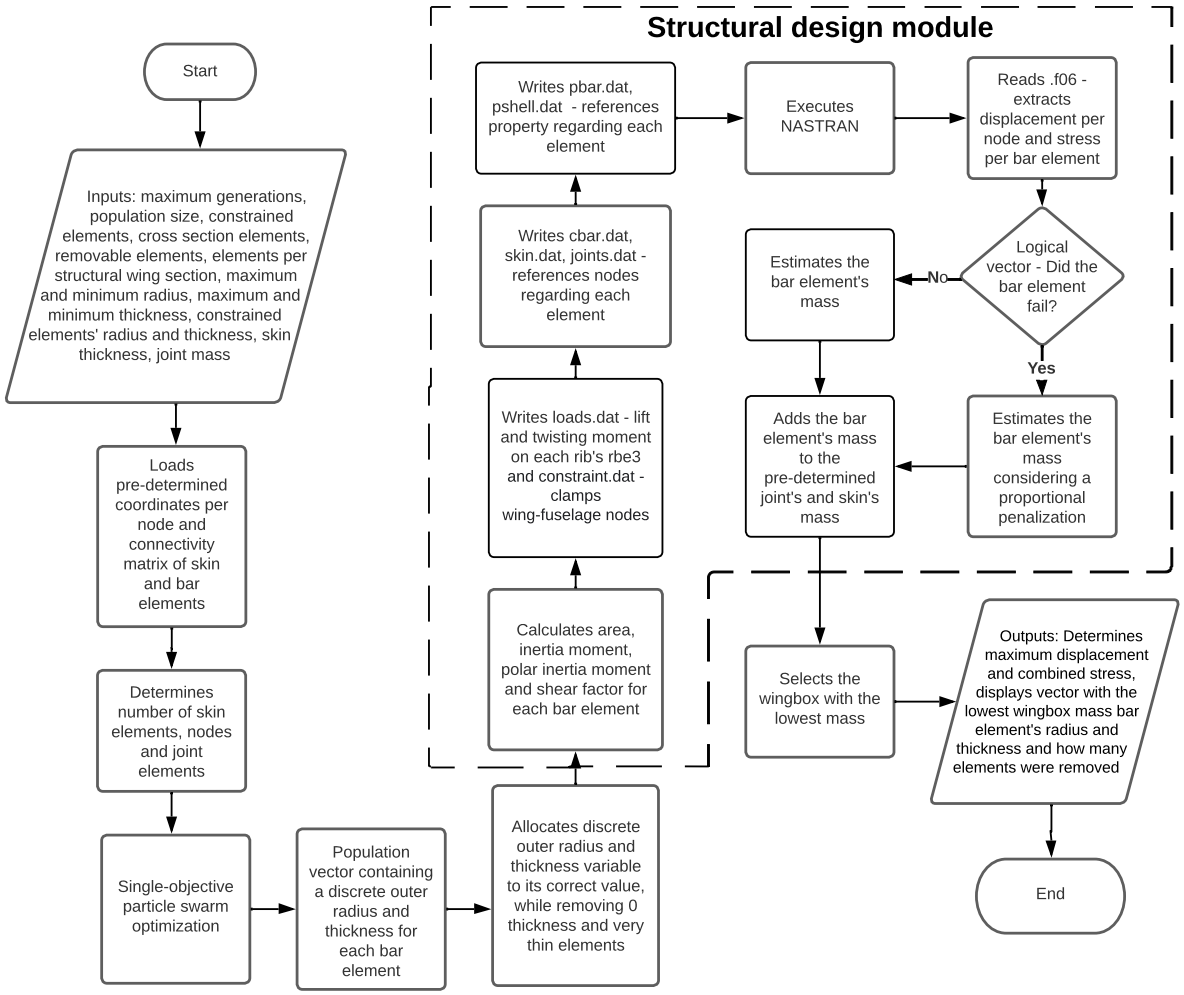

Figure 8: Flowchart of the optimization process.

4. RESULTS

4.1 Loads

As discussed in Subsection 2.2 the lift coefficient, lift force, and twisting moment acting on the wing in the cruise condition were calculated by the fixed-speed VLM1 analysis and distributed throughout each of the wingbox's truss-based ribs' aerodynamic centers. The results were obtained for an angle of attack of 0°, considered as a hypothesis for the cruise trimmed condition. Given that, the resulting distributions are depicted in Figures 9a, 9b, and 9c, respectively, whereupon each marker represents a truss-based rib of the wingbox.

Furthermore, with all boundary conditions determined, the loads were applied to the structural model, as displayed in Figure 10.

4.2 Optimization Results

First and foremost, the inputs specified in Figure 8 for the single-objective particle swarm optimization had to be determined. The number of variables was set as double the amount of optimizable trusses, since the algorithm optimizes both their outer radius and thicknesses. It is worth noting that the number of optimizable trusses is smaller than the number of trusses in the FEM, because clamped trusses had a fixed outer radius and thickness, since both their nodes could not be displaced. In addition, the elements needed to maintain minimum aerodynamic profile were specified, since they could not be removed.

Furthermore, the discrete values for outer radius and thickness were defined. As proposed by Silva *et al.* (2022),

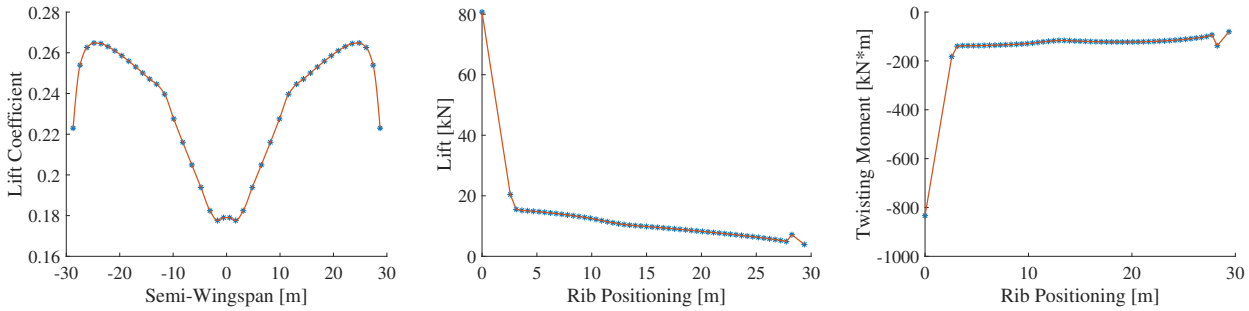

(a) Lift coefficient distribution. (b) Lift distribution. (c) Twisting Moment distribution.

Figure 9: Loads obtained for the cruise condition.

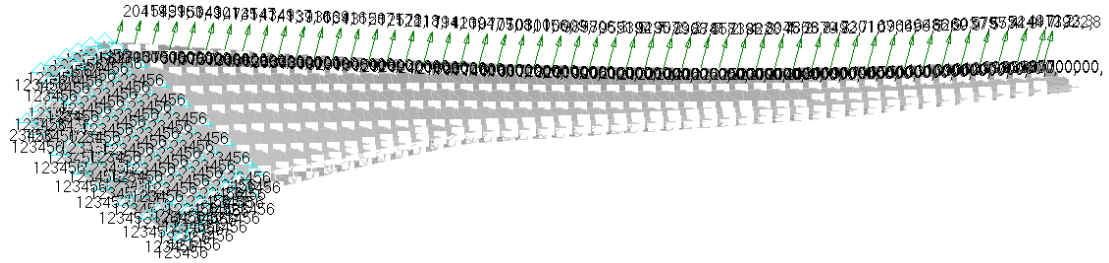

Figure 10: Loads and constraints applied to the FEM.

outer radius values were evenly spaced by 5 mm, while thickness values by 2 mm. The maximum and minimum outer radius, as well as the maximum and minimum thickness, both varied according to each structural wingbox section's expected structural response, with the maximum outer radius decreasing by 5 mm in each section from root to tip and the maximum thickness decreasing by 2 mm in each section from root to tip. Nevertheless, both the minimum outer radius and thickness were constant throughout the sections. Additionally, even though the thickness of the skin panels was maintained at 2,25 mm, since it isn't part of the optimization process, it is fitted to the best possible result. Also, the mass of each joint was set at 150 g ((Silva *et al.*, 2022)).

The optimization process' population size was initially set at 100, given that, over the course of the development of this work, it was noticed that a smaller number of individuals per iteration wouldn't hinder the optimization process, whilst allowing it to converge faster, i.e., the optimization process benefited from a high number of iterations rather than population size. Nonetheless, at 2000 iterations, the result displayed signs of convergence, exhibiting the need of an increase in population size, with a swarm size increment to 500. Finally, all inputs that were needed to run this sample result's cycle can be seen in Table 8.

Table 8: Optimization parameters.

Parameter	Value
Number of variables	5460
Constrained trusses	453
Constrained trusses' outer radius	5 mm
Constrained trusses' thickness	1 mm
Optimizable trusses	2730
Trusses with possible removal	1051
Skin's thickness	2,25 mm
Joint's mass	150 g
Iterations	2000 - 1700
Population size	100 - 500

$$\begin{cases} \min\left(W_{wing}\right) \\ \mathbf{x} : [D_{i_{\text{ext,tube}}}, t_{i_{\text{tube}}}] \quad \text{for } i = 1, 2, \ldots, N_{\text{truss elements}} \\ D_{i_{\text{ext,tube}}} = 10{,}15{,}20{,}\ldots{,}120 \quad [\text{mm}] \\ t_{i_{\text{tube}}} = 2{,}4{,}6{,}\ldots{,}44 \quad [\text{mm}] \end{cases}$$

Given the inputs to run the cycle, the outputs specified in Figure 8 could be obtained and displayed in Table 9, and the evolution of the function value over the iterations is shown in Figure 11. Additionally, the wingbox's displacement may be observed in Figure 12, while its removed elements are highlighted in red in Figure 13.

Table 9: Optimization results.

Parameter	Value
Total time	20 days and 6 hours
Number of elements removed	282
Maximum displacement	1772.53 mm
Maximum combined stress	366.39 MPa
Minimum wing weight	12.38 ton

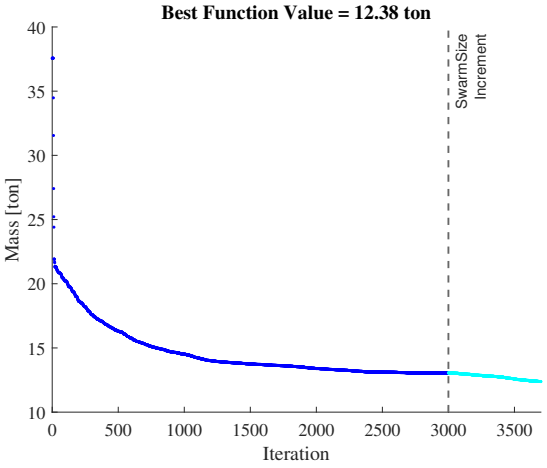

Figure 11: Optimization convergence.

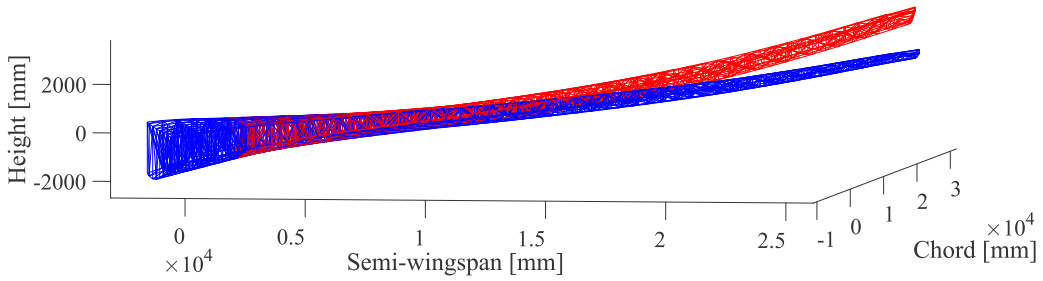

Figure 12: Wingbox's displacement.

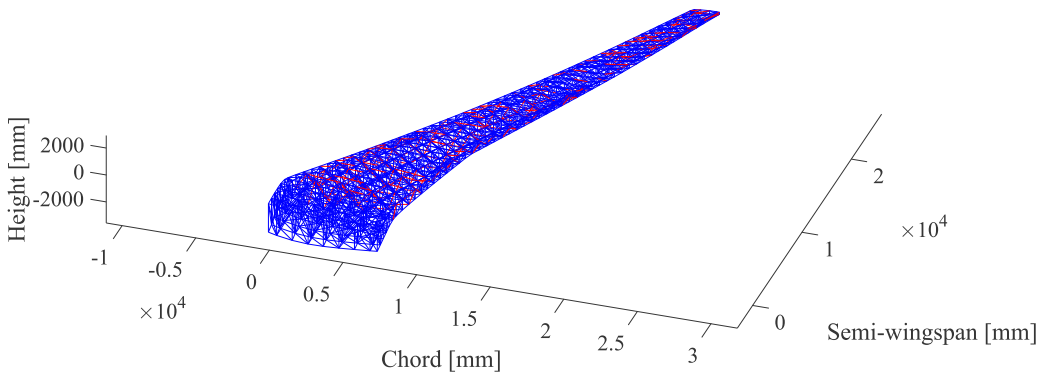

Figure 13: Wingbox's removed elements.

The total time of 20 days and 6 hours, through the course of both steps of the optimization process, initially at 100 and later at 500 population size, shows that each individual takes about 2.69 seconds to be optimized. Additionally, 282 trusses were removed (26.83%), those considered unnecessary for both the aerodynamic profile and structural integrity, allowing to optimize the wingbox's empty weight while staying inside the safety factor, with no penalized trusses. Given this is a research in development, the global minimum has not yet been found, as the lack of convergence in the last iterations tell, with another future increase in population size possible, given that its last increment, although computationally costly (from 277 s to 1345 s per iteration), descreased the wing's weight in 0,67 tons, while still not displaying signs of convergence.

Finally, Table 10 displays the wingbox's mass distribution, whereupon the trusses account for 13.27 ton (91.8%) of the total empty weight. Hence, the optimization of the skin panels' thickness and a different value of joint mass as the one proposed by Silva *et al.* (2022) could decrease the wingbox's empty weight to an even lower value. Nevertheless, the optimized truss-based NASA CRM wingbox still managed to be 17.8% lighter when compared to the original wing weight (Table 6).

Table 10: Wingbox's mass distribution.

Component	Weight [ton]
Trusses	11.37
Skin panels	0.9
Joints	0.11

4.3 Buckling Post-Analysis

After obtaining the optimized wing design, a post-analysis was conducted to assess the buckling behavior and ensure the structural integrity of the wingbox. NASTRAN's SOL106 was used for this purpose. The post-analysis involved determining the first five eigenvalues using Lanczos' solution method, and the corresponding results are presented in Table 3. The critical instability of the wingbox associated with eigenvalue #1 is visualized in Figure 14.

Table 11: Buckling results.

Eigenvalue #	Value
1	12.86
2	13.18
3	-18.84
4	-21.66
5	-25.45

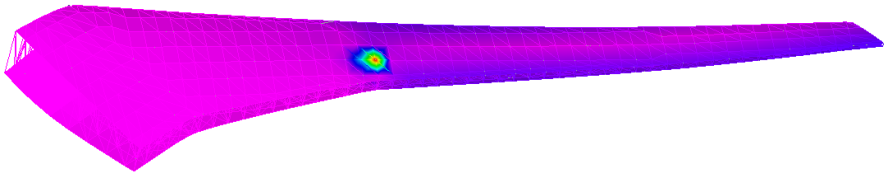

Figure 14: Buckling analysis (eigenvalue #1).

As evident from the results, the optimized wingbox demonstrates significant structural integrity, as it remains well below the critical buckling limit when subjected to the applied loads. Therefore, the wingbox is deemed structurally stable and capable of withstanding the given load conditions without buckling failure.

5. CONCLUDING REMARKS

This paper presents a new wing design approach. It assesses the concept of a truss-based modular internal wingbox structure applied to a large-scale commercial aircraft model, which is the NASA's Common Research Model. The results showed that the proposal can be a good strategy in structural design, even with its limitations.

Firstly, the truss-based modular structure wingbox, optimized using a particle swarm optimization algorithm, demonstrated a lighter weight compared to the original CRM wingbox, despite having not yet converged. This outcome highlights the effectiveness of this innovative approach in designing the inner structures of the wingbox, particularly in the context of alternative propulsion systems.

Furthermore, a thorough buckling post-analysis confirmed the structural integrity of the optimized wingbox, indicating that it can withstand the applied loads without experiencing buckling failure. This analysis also identified potential opportunities for optimizing the thickness of the skin panels, thereby providing scope for further weight reduction and improved performance.

Finally, there are still great potential for developing improvements in the structural model, such as a more optimized spatial arrangement of the structural mesh - with the optimization of the number and position of the truss-based ribs and its truss sections - and the integrated buckling optimization of skin elements. The evaluation of uncertainties in the manufacturing of the composite plates and tubes and an assessment of a TBW structure - envisaging easing manufacturing issues and analyzing the wing-fuselage connection elements - should also enhance the structural project of this wingbox. Additionally, an aeroelastic model evaluating the behavior of the resulting wingbox structure would aid in verifying structural integrity, given flutter and divergence speeds. Similarly, the evaluation of the wingbox under extreme loads, determined through its V-n diagram, is recommended. Due to the large number of design variables in the optimization, the computational time is still a big challenge.

6. REFERENCES

Aerovintage, 2022. "B-17G Champaign Lady Update: 02/18/2022". `https://www.aerovintage.com/2022/02/18/b-17g-champaign-lady-update-02-18-2022/`. Last access on 2023-09-04.

Bai, Y. and Yang, X., 2013. "Novel joint for assembly of all-composite space truss structures: conceptual design and preliminary study". *Journal of Composites for Construction*, Vol. 17, No. 1, pp. 130–138.

Bhatia, M., Kapania, R., van Hoek, M. and Haftka, R., 2009. "Structural design of a truss braced wing: potential and challenges". In *50th AIAA/ASME/ASCE/AHS/ASC Structures, Structural Dynamics, and Materials Conference 17th AIAA/ASME/AHS Adaptive Structures Conference 11th AIAA No*. p. 2147.

Bhatia, M., Kapania, R.K. and Haftka, R.T., 2012. "Structural and aeroelastic characteristics of truss-braced wings: A parametric study". *Journal of Aircraft*, Vol. 49, No. 1, pp. 302–310.

Cavalini Jr, A.A., Lobato, F.S., Koroishi, E.H. and Steffen Jr, V., 2016. "Model updating of a rotating machine using the self-adaptive differential evolution algorithm". *Inverse Problems in Science and Engineering*, Vol. 24, No. 3, pp. 504–523.

Coggin, J.M., Kapania, R.K., Schetz, J.A., Vijayakumari, H. and Zhao, W., 2014. "Nonlinear aeroelastic analysis of a truss based wing aircraft". In *55th AIAA/ASMe/ASCE/AHS/SC Structures, Structural Dynamics, and Materials Conference*. p. 0335.

Finistauri, A.D., Xi, F. and Walsh, P., 2012. "Discretization method for the development of a modular morphing wing". *Journal of Aircraft*, Vol. 49, No. 1, pp. 116–125.

Friedrich, C. and Robertson, P.A., 2015. "Hybrid-electric propulsion for aircraft". *Journal of Aircraft*, Vol. 52, No. 1, pp. 176–189.

Fujiwara, G.E., Nguyen, N.T., Livne, E. and Bragg, M.B., 2018. "Aerostructural design optimization of a flexible wing aircraft with continuous morphing trailing edge". In *2018 Multidisciplinary Analysis and Optimization Conference*. p. 3571.

Gern, F.H., Naghshineh-Pour, A.H., Sulaeman, E., Kapania, R.K. and Haftka, R.T., 2001. "Structural wing sizing for multidisciplinary design optimization of a strut-braced wing". *Journal of aircraft*, Vol. 38, No. 1, pp. 154–163.

Graham, W.R., Hall, C.A. and Morales, M.V., 2014. "The potential of future aircraft technology for noise and pollutant emissions reduction". *Transport policy*, Vol. 34, pp. 36–51.

Guimaraes, T., Pereira, D., de Mello, W. and Rade, D., 2017. "Uncertainty propagation and optimization of the dynamic behavior of tow steered composite plates". In *Proceedings of the International Conference on Structural Engineering Dynamics*.

Guimarães, T.A., Castro, S.G., Rade, D.A. and Cesnik, C.E., 2017. "Panel flutter analysis and optimization of composite tow steered plates". In *58th AIAA/ASCE/AHS/ASC structures, structural dynamics, and materials conference*. p. 1118.

Guimarães, T.A., Castro, S.G., Cesnik, C.E. and Rade, D.A., 2019. "Supersonic flutter and buckling optimization of tow-steered composite plates". *AIAA Journal*, Vol. 57, No. 1, pp. 397–407.

Jutte, C.V., Stanford, B., Wieseman, C.D. and Moore, J.B., 2014. "Aeroelastic tailoring of the nasa common research model via novel material and structural configurations". In *52nd aerospace sciences meeting*. p. 0598.

Kenway, G., Kennedy, G. and Martins, J.R., 2014. "Aerostructural optimization of the common research model configuration". In *15th AIAA/ISSMO multidisciplinary analysis and optimization conference*. p. 3274.

Lacy, D.S. and Sclafani, A.J., 2016. "Development of the high lift common research model (hl-crm): A representative high lift configuration for transonic transports". In *54th AIAA aerospace sciences meeting*. p. 0308.

Mallik, W., Kapania, R.K. and Schetz, J.A., 2013. "Multidisciplinary design optimization of medium-range transonic truss-braced wing aircraft with flutter constraint". In *54th AIAA/ASME/ASCE/AHS/ASC Structures, Structural Dynamics, and Materials Conference*. p. 1454.

Masiol, M. and Harrison, R.M., 2014. "Aircraft engine exhaust emissions and other airport-related contributions to ambient air pollution: A review". *Atmospheric Environment*, Vol. 95, pp. 409–455.

Mesogitis, T., Skordos, A.A. and Long, A., 2014. "Uncertainty in the manufacturing of fibrous thermosetting composites: A review". *Composites Part A: Applied Science and Manufacturing*, Vol. 57, pp. 67–75.

Petrescu, R.V.V., Machin, A., Fontanez, K., Arango, J.C., Marquez, F.M. and Petrescu, F.I.T., 2020. "Hydrogen for aircraft power and propulsion". *international journal of hydrogen energy*, Vol. 45, No. 41, pp. 20740–20764.

Pornet, C. and Isikveren, A.T., 2015. "Conceptual design of hybrid-electric transport aircraft". *Progress in Aerospace Sciences*, Vol. 79, pp. 114–135.

Rivers, M.B., 2019. "Nasa common research model: a history and future plans". In *AIAA Aviation 2019 Forum*. p. 3725.

Rivers, M.B., Lynde, M.N., Campbell, R.L., Viken, S.A., Chan, D.T., Watkins, A.N. and Goodliff, S.L., 2019. "Experimental investigation of the nasa common research model with a natural laminar flow wing in the nasa langley national transonic facility". In *AIAA Scitech 2019 Forum*. p. 2189.

Sgueglia, A., Schmollgruber, P., Bartoli, N., Benard, E., Morlier, J., Jasa, J., Martins, J.R., Hwang, J.T. and Gray, J.S., 2020. "Multidisciplinary design optimization framework with coupled derivative computation for hybrid aircraft".

Journal of Aircraft, Vol. 57, No. 4, pp. 715–729.

Silva, H.L., Resende, G.J., Neto, R.M., Carvalho, A.R., Gil, A.A., Cruz, M.A. and Guimarães, T.A., 2021. "A multi-disciplinary design optimization for conceptual design of hybrid-electric aircraft". *Structural and Multidisciplinary Optimization*, Vol. 64, No. 6, pp. 3505–3526.

Silva, H.L., Guimarães, T.A. and Castro, S.G., 2023. "Design and aeroelastic analysis of truss-based modular wing structures". In *AIAA SCITECH 2023 Forum*. p. 1677.

Silva, H.L. *et al.*, 2022. "Structural and aeroelastic design optimization of truss-based modular wing structures".

Stanford, B.K. and Jutte, C.V., 2017. "Comparison of curvilinear stiffeners and tow steered composites for aeroelastic tailoring of aircraft wings". *Computers & Structures*, Vol. 183, pp. 48–60.

Stanford, B.K., Jutte, C.V. and Wu, K.C., 2014. "Aeroelastic benefits of tow steering for composite plates". *Composite Structures*, Vol. 118, pp. 416–422.

Starnes Jr, J.H. and Haftka, R.T., 1979. "Preliminary design of composite wings for buckling, strength, and displacement constraints". *Journal of Aircraft*, Vol. 16, No. 8, pp. 564–570.

Tang, D., Chen, L., Hu, E. and Tian, Z.F., 2016. "A novel actuator controller: Delivering a practical solution to realization of active-truss-based morphing wings". *IEEE Transactions on Industrial Electronics*, Vol. 63, No. 10, pp. 6226–6237.

Vassberg, J., Dehaan, M., Rivers, M. and Wahls, R., 2008. "Development of a common research model for applied cfd validation studies". In *26th AIAA applied aerodynamics conference*. p. 6919.

Vassberg, J.C., 2012. "Airfoil geometry: Camber and thickness distributions".

Ye, J., Kyvelou, P., Gilardi, F., Lu, H., Gilbert, M. and Gardner, L., 2021. "An end-to-end framework for the additive manufacture of optimized tubular structures". *IEEE Access*, Vol. 9, pp. 165476–165489.

7. RESPONSIBILITY NOTICE

The authors are solely responsible for the printed material included in this paper.